A new solution to a weakly non-linear heat conduction equation in a spherical droplet: Basic idea and applications

Dmitrii V. Antonov [a,c], Elena A. Shchepakina [b], Vladimir A. Sobolev [b], Elena M. Starinskaya [c], Vladimir V. Terekhov [c], Pavel A. Strizhak [a], Sergei S. Sazhin [c,d,*]

[a] *Heat and Mass Transfer Laboratory, National Research Tomsk Polytechnic University, 30 Lenin Avenue, Tomsk 634050, Russian Federation*
[b] *Samara National Research University, 34 Moskovskoye Shosse, Samara 443086, Russian Federation*
[c] *Kutateladze Institute of Thermophysics Siberian Branch, Russian Academy of Sciences, 1 Lavrentiev Avenue, Novosibirsk 630090, Russian Federation*
[d] *Advanced Engineering Centre, School of Architecture, Technology and Engineering, University of Brighton, Brighton, BN2 4GJ, UK*

ARTICLE INFO

ABSTRACT

A new analytical solution to a non-linear heat transfer equation in a spherically-symmetric droplet is suggested. All thermophysical properties inside the droplet are considered to be close to their average values. This allows us to consider the non-linearity of this equation as weak. The solution is presented as $T = T_0 + T_1$, where T_0 is the solution to a linear heat conduction equation, and $T_1 \ll T_0$. The equation for T_1 is presented as a linear heat conduction equation with a source term depending on the distribution of T_0 and its spatial derivatives inside the droplet. The latter equation is solved analytically alongside the linear equation for T_0, and the final solution is presented as $T = T_0 + T_1$. The predictions of the numerical code in which this solution was implemented are verified based on a comparison of those predictions with the predictions of COMSOL Multiphysics code using input parameter values that are typical for nanofluid (water and SiO_2 nanoparticles) droplet evaporation in atmospheric conditions. It is demonstrated that for these experiments $T_1 \ll T_0$ which justifies the applicability of the linear heat conduction equation used for the analysis of this process. Small differences in the temperatures predicted by both non-linear and linear models lead to a much more noticeable difference in integral characteristics such as time before the start of the formation of the cenosphere when the mass fraction of nanoparticles at the droplet surface reaches about 40%.

1. Introduction

The importance of modelling mono- and multi-component droplet heating and evaporation for various applications has been commonly recognised, and various approaches to this problem have been discussed in numerous papers, the results of which are summarised in many monographs, including [1–5], and reviews, including [6,7]. Interesting discussions of this problem are presented in [8–10].

In the case of spherical droplets, we believe that one of the promising approaches to this problem is based on the implementation of the analytical solutions to the heat conduction and component diffusion equations in the liquid phase into a numerical code and using these solutions at each timestep of the analysis [5]. This approach was used in our most recent paper focused on this problem [11], in which a new model for mono-component droplet heating/evaporation was developed, tested, and applied to the analysis of in-house experimental data.

The new model linked the previously developed liquid phase model, using the analytical solution to the heat transfer equation at each timestep [5], and the gas phase model, using the solution to the equations of the conservation of mass, momentum, and energy, leading to an explicit expression for the Nusselt number and implicit expression for evaporation rate of the droplet [12].

One of the key limitations of this approach is that it is based on the assumption that the heat conduction equation in the liquid phase is linear. This means that all liquid thermophysical properties used in this equation are assumed to be the same throughout the whole droplet volume. The validity of this assumption has never been investigated to the best of our knowledge. We anticipate that this assumption is acceptable in the case of mono-component droplets, remembering that liquid thermodynamic and transport properties are weak functions of temperature, and the temperature variations inside droplets are small in most applications [5].

Nomenclature

a	$\sqrt{k_{l0}/(\rho_{l0}c_{l0})}$ .... m/$\sqrt{\text{s}}$	
A_n	symbol introduced in (36)	
b	h/k_{l0} 1/m	
B_M	Spalding heat transfer number	
c	specific heat capacity .... J/(kg K)	
D	diffusion coefficient .... m^2/s	
G	Green function	
h	convective heat transfer coefficient .... W/(m^2 K)	
k	thermal conductivity .... W/(m K)	
L	heat of evaporation .... J/kg	
Q_0	parameter defined by Expression (15) .... K	
P	source term .... W/m^3	
R	distance from the droplet centre .... m	
R_d	droplet radius .... m	
t	time .... s	
T	temperature .... K	
Y	mass fraction	

Greek symbols

ε_i	$\dfrac{Y_{vis}}{\sum_i Y_{vis}}$	
μ_n	eigenvalues	
ν	$\dfrac{k_{l0}}{\rho_{l0}c_{l0}R_d^2}$ 1/s	
ρ	density .... kg/m^3	

Subscripts

e	evaporation
d	droplet
eff	effective
g	ambient gas
i	component
l	liquid
s	surface
total	vapour + air
0	initial or zeroth order
1	end of the timestep or first order

For multi-component droplets, however, this assumption can be questionable, as thermodynamic and transport properties of components can differ considerably and the mass fractions of components in different parts of the droplets (e.g. centre and surface) can vary from being close to zero to being close to one. The challenges of developing non-linear models are well known [13–16] and most researchers try to avoid these models especially for engineering applications. However, even in the case of multi-component droplets the solutions to linear and non-linear heat conduction equations are expected to be reasonably close (this is supported by the results presented in paper), and this closeness supports the development of a new approach to solving the equation, based on the assumption that it is weakly non-linear. This assumption will be justified based on the application of our results to a practical engineering problem.

The focus of the paper is on obtaining a new analytical solution to a weakly non-linear heat conduction equation, and implementation of this solution into a numerical code alongside the previously obtained analytical solutions to the component diffusion equations and the model for droplet evaporation and swelling. The predictions of this new code will be compared with those of the previously developed numerical code based on the analytical solution to the linear heat conduction equation for input parameter values that are typical during the evaporation of nanofluid droplets.

Note that the idea of developing a weakly non-linear model is not new. Such models have been developed for various applications in physics and engineering (e.g. [17], where the linear interaction analysis is used to study the shock-turbulence interaction in supersonic and hypersonic flows). We believe, however, that this is the first model of this kind to be developed for the analysis of droplet heating and evaporation. The range of applicability of the new model is certainly not limited to the analysis of nanofluid droplets (see [5] for an extensive analysis of other types of multi-component droplets).

The key equations on which the model is based and the new solution to the weakly non-linear heat conduction equation are described in Section 2. The main features of the numerical algorithm used in the analysis are summarised in Section 3. The predictions of the newly developed numerical code are verified in Section 4 based on a comparison of its predictions with the predictions of COMSOL Multiphysics code. The predictions of the new code and the previously developed version (based on the analytical solution to the linear heat conduction equation in the droplet) are compared in Section 5. The main results of the paper are summarised in Section 6.

2. Basic equations and approximations

2.1. Heat transfer equation

Assuming the spherical symmetry of the problem, the heat transfer equation inside a droplet can be presented as [18,19]

$$\rho_l c_l \frac{\partial T}{\partial t} = \frac{1}{R^2} \frac{\partial}{\partial R}\left(R^2 k_l \frac{\partial T}{\partial R}\right), \qquad (1)$$

where ρ_l, c_l, and k_l are the density, specific heat capacity and thermal conductivity of a liquid, respectively, T is temperature, t is time, R is the distance from the droplet centre. $0 \le t < \infty$, $0 \le R \le R_d$, where R_d is the droplet radius.

Several analytical solutions to this equation, subject to various boundary and initial conditions were obtained in [5]. These solutions were incorporated into numerical codes and used for the analysis of droplet heating, evaporation, puffing and micro-explosions [5].

In all these solutions, however, it was assumed that ρ_l, c_l, and k_l are constant during each timestep (they do not depend on t and R).[1] That means that the analysis was focused on a linear problem. References to some papers where this assumption is relaxed are given in the preface to [5], but this case is not investigated in the book.

At the same time, this assumption turned out to be rather restrictive in many practical applications. For example, at the final stages of nanofluid droplet drying all three parameters, ρ_l, c_l, and k_l, are expected to depend on R due to the accumulation of nanoparticles near the droplet surface [20].

We do not intend to solve a general non-linear version of Equation (1). Instead, our focus will be on the solution of a weakly non-linear problem in which ρ_l, c_l, k_l, and T are presented as:

$$\rho_l(R) = \rho_{l0} + \rho_{l1}(R), \quad c_l(R) = c_{l0} + c_{l1}(R), \quad k_l(R) = k_{l0} + k_{l1}(R),$$

$$T(R) = T_0(R) + T_1(R), \qquad (2)$$

where ρ_{l0}, c_{l0}, and k_{l0} are average values of density, specific heat capacity and the thermal conductivity of liquid, respectively, which are assumed to be constant during each timestep; c_{l1}, c_{l1}, and k_{l1} are perturbations to ρ_{l0}, c_{l0}, and k_{l0}, respectively, which depend on R at each timestep. It is assumed that

---

[1] For composite droplets they were assumed to be constant in *a priori* chosen ranges of R (see [5]).

$$|\rho_{l1}| \ll |\rho_{l0}|, \quad |c_{l1}| \ll |c_{l0}|, \quad |k_{l1}| \ll |k_{l0}|. \tag{3}$$

T_0 is the solution to (1) assuming that $\rho_l = \rho_{l0}$, $c_l = c_{l0}$, and $k_l = k_{l0}$.

It is anticipated that Conditions (2)-(3) imply that

$$T_1 \ll T_0. \tag{4}$$

The substitution of (2) into (1) allows us to re-write the latter equation as:

$$\left(\rho_{l0}c_{l0} + \rho_{l0}c_{l1} + \rho_{l1}c_{l0}\right)\frac{\partial(T_0 + T_1)}{\partial t}$$
$$= \frac{1}{R^2}\frac{\partial}{\partial R}\left(R^2(k_{l0} + k_{l1})\frac{\partial(T_0 + T_1)}{\partial R}\right). \tag{5}$$

When deriving (5) Conditions (3) were used. The term $\rho_{l1}c_{l1}$ was removed from the left-hand side of (5) as this term is of a higher order of magnitude than the terms $\rho_{l0}c_{l1}$ and $\rho_{l1}c_{l0}$. Note that the contribution of this term could be considered by adding it to $(\rho_{l0}c_{l1} + \rho_{l1}c_{l0})$ in the final solution.

Remembering that T_0 satisfies the equation:

$$\rho_{l0}c_{l0}\frac{\partial T_0}{\partial t} = \frac{1}{R^2}\frac{\partial}{\partial R}\left(R^2 k_{l0}\frac{\partial T_0}{\partial R}\right) = k_{l0}\left(\frac{\partial^2 T_0}{\partial R^2} + \frac{2}{R}\frac{\partial T_0}{\partial R}\right). \tag{6}$$

Equation (5) can be simplified to:

$$\rho_{l0}c_{l0}\frac{\partial T_1}{\partial t} + \left(\rho_{l0}c_{l1} + \rho_{l1}c_{l0}\right)\frac{\partial T_0}{\partial t} =$$
$$k_{l0}\frac{\partial^2 T_1}{\partial R^2} + k_{l1}\frac{\partial^2 T_0}{\partial R^2} + \frac{2k_{l0}}{R}\frac{\partial T_1}{\partial R} + \left[\frac{1}{R^2}\frac{\partial(R^2 k_{l1})}{\partial R}\right]\frac{\partial T_0}{\partial R}. \tag{7}$$

Equation (7) can be further simplified to

$$\rho_{l0}c_{l0}\frac{\partial T_1}{\partial t} = k_{l0}\left(\frac{\partial^2 T_1}{\partial R^2} + \frac{2}{R}\frac{\partial T_1}{\partial R}\right) + P(R), \tag{8}$$

where

$$P(R) = -\left(\rho_{l0}c_{l1} + \rho_{l1}c_{l0}\right)\frac{\partial T_0}{\partial t} + k_{l1}\frac{\partial^2 T_0}{\partial R^2} + \left[\frac{1}{R^2}\frac{\partial(R^2 k_{l1})}{\partial R}\right]\frac{\partial T_0}{\partial R}. \tag{9}$$

The known solution to Equation (6) and known dependencies of ρ_{l1}, c_{l1}, and k_{l1} on R allow us to calculate the value of $P(R)$ based on Expression (9). Once the term $P(R)$ has been obtained, the solution to the linear heat conduction equation with the source term described in [5] can be used to solve (8) after replacing T with T_1. This solution for *a priori* known P, subject to the initial and boundary conditions (11) and (13), is presented in Appendix A.

The initial conditions for Equations (6) and (8) are the standard ones:

$$T_0(R)(t = 0) = T_{00}(R), \quad T_1(R)(t = 0) = 0. \tag{10}$$

At the second and the following timesteps

$$T_{00}(R) = T_0(R)(t = t_1) + T_1(R)(t = t_1),$$

where $T_0(R)(t = t_1)$ and $T_1(R)(t = t_1)$ are the solutions at the previous timestep with possibly modified values of the input parameters. In what follows, no indication is made of the dependence of these parameters on R.

The Robin boundary condition for Equations (6) and (8) at the droplet surface is used. It takes the form:

$$\left[(k_{l0} + k_{l1})\left(\frac{\partial T_0}{\partial R} + \frac{\partial T_1}{\partial R}\right) + h(T_0 + T_1)\right]\Bigg|_{R=R_d-0} = hT_g(t), \tag{11}$$

where h is the convection heat transfer coefficient (see [21] for the details of its estimation), R_d is the droplet radius, T_g is ambient gas temperature.

Thus, we have the boundary conditions for T_0:

$$\left[k_{l0}\frac{\partial T_0}{\partial R} + hT_0\right]\Bigg|_{R=R_d-0} = hT_g(t), \tag{12}$$

and T_1:

$$\left[k_{l0}\frac{\partial T_1}{\partial R} + hT_1\right]\Bigg|_{R=R_d-0} = -\left[k_{l1}\frac{\partial T_0}{\partial R}\right]\Bigg|_{R=R_d-0},$$

or

$$\left[k_{l0}\frac{\partial T_1}{\partial R} + hT_1\right]\Bigg|_{R=R_d-0} = -\left[\frac{hk_{l1}}{k_{l0}}\left(T_g(t) - T_0\right)\right]\Bigg|_{R=R_d-0}. \tag{13}$$

Note that the contribution of the higher order term $k_{l1}\frac{\partial T_1}{\partial R}$ in (13) has been ignored.

2.2. Analytical solutions

The solution presented in Appendix A formally solves the problem for T_1 after the source term P has been obtained based on Expression (9). In this section an alternative analytical solution to the problem is presented which turned out to be more convenient for numerical analysis. Alternative analytical solutions to Equations (6) and (8) follow from the solution to an auxiliary problem solved in Appendix B (Expression (41)).

Assuming that

$$u = T_0, \quad a^2 = \frac{k_{l0}}{\rho_{l0}c_{l0}}, \quad F(R,s) = 0, \quad f(R) = T_{00}(R),$$
$$H(t) = H_0(t) = T_g(t), b = h/k_{l0}$$

in Expression (41), the latter expression gives us the explicit formula for T_0 (zeroth approximation):

$$T_0(R,t) = Q_0(R,t) + \frac{1}{R}\int_0^{R_d} G(R,r,t)rT_{00}(r)dr, \tag{14}$$

where

$$Q_0(R,t) = T_g(t) - \frac{2}{RR_d}\sum_{n=1}^{\infty} A_n \sin\left(\mu_n\frac{R}{R_d}\right)\left(\frac{R_d}{\mu_n}\right)^2 \frac{hR_d}{k_{l0}}\sin(\mu_n)$$
$$\times\left[T_g(t) - \nu\mu_n^2\int_0^t T_g(s)\exp\left(-\nu\mu_n^2(t-s)\right)ds\right], \tag{15}$$

$$G(R,r,t) = \frac{2}{R_d}\sum_1^{\infty} A_n \sin\left(\mu_n\frac{R}{R_d}\right)\sin\left(\mu_n\frac{r}{R_d}\right)\exp\left(-\nu\mu_n^2 t\right),$$

and

$$\nu = \frac{k_{l0}}{\rho_{l0}c_{l0}R_d^2} = \frac{a^2}{R_d^2}.$$

Symbol A_n is introduced in (36).

Expression (14) can be re-written as

$$T_0(R,t) = Q_0(R,t) + \frac{1}{R}\frac{2}{R_d}$$
$$\times\sum_{n=1}^{\infty} A_n \sin\left(\mu_n\frac{R}{R_d}\right)\exp\left(-\nu\mu_n^2 t\right)\int_0^{R_d}\sin\left(\mu_n\frac{r}{R_d}\right)rT_{00}(r)dr. \tag{16}$$

Note that the integral in (15) can be rearranged using the following formula, which we found useful for numerical calculations:

$$\nu\mu_n^2\int_0^t T_g(s)\exp\left(-\nu\mu_n^2(t-s)\right)ds = \nu\mu_n^2\exp\left(-\nu\mu_n^2 t\right)$$
$$\times\int_0^t T_g(s)\exp\left(\nu\mu_n^2 s\right)ds.$$

Formulae (14) and (16) reduce to Expression (23) with $P = 0$, which is equivalent to Expression (2.41) of [5] (see Appendix C for the details).

Having introduced the following parameters and functions

$$u = T_1, \quad F(R) = \frac{P(R)}{\rho_{l0} c_{l0}}, \quad f(R) = 0,$$

$$H(t) = H_1(t) = -\frac{k_{l1}}{k_{l0}} \left[T_g(t) - T_0 \big|_{R=R_d-0} \right],$$

Expression (41) gives us the explicit formula for T_1:

$$T_1(R,t) = Q_1(R,t) + \frac{1}{R} \int_0^t \int_0^{R_d} G(R,r,t-s) r \frac{P(r)}{\rho_{l0} c_{l0}} dr ds, \qquad (17)$$

where

$$Q_1(R,t) = H_1(t) - \frac{2}{RR_d} \sum_{n=1}^{\infty} A_n \sin\left(\mu_n \frac{R}{R_d}\right) \left(\frac{R_d}{\mu_n}\right)^2 b R_d \sin(\mu_n)$$

$$\times \left[H_1(t) - \nu \mu_n^2 \int_0^t H_1(s) \exp\left(-\nu\mu_n(t-s)\right) ds \right] =$$

$$H_1(t) - \frac{2}{RR_d} \sum_1^{\infty} A_n \sin\left(\mu_n \frac{R}{R_d}\right) \left(\frac{R_d}{\mu_n}\right)^2 b R_d \sin(\mu_n)$$

$$\times \left[H_1(t) - \nu \mu_n^2 \exp\left(-\nu\mu_n^2 t\right) \int_0^t H_1(s) \exp\left(\nu\mu_n^2 s\right) ds \right],$$

$P(R)$ is given by Expression (9), the Green function G is given by Expression (38), eigenvalues μ_n are solutions to Equation (24).

The effect of droplet evaporation is considered by replacing T_g with

$$T_{\text{eff}} = T_g + \rho_l L \dot{R}_{d(e)} h^{-1},$$

where $\dot{R}_{d(e)} = \frac{dR_d}{dt}$ describes the contribution of evaporation. The latter process is modelled using the approach described by Abramzon and Sirignano [21].

The change in droplet radius due to thermal swelling and evaporation was taken into account during the transition between timesteps.

The effect of a support (wire) on droplet heating was considered assuming that this effect is small and heat supplied or taken by the support is homogeneously and instantaneously distributed throughout the whole droplet volume [22].

2.3. Component diffusion

For multi-component liquid, the following equations for mass fractions of components $Y_{li} \equiv Y_{li}(t,R)$ ($0 \leq Y_{li} \leq 1$)

$$\frac{\partial Y_{li}}{\partial t} = D_l \left(\frac{\partial^2 Y_{li}}{\partial R^2} + \frac{2}{R} \frac{\partial Y_{li}}{\partial R} \right), \qquad (18)$$

where D_l is the component diffusivity, $i \geq 1$, were solved analytically subject to boundary and initial conditions [5]:

$$\frac{\partial Y_{li}}{\partial R} \bigg|_{R=R_d-0} = \frac{D_v \rho_{\text{total}} \ln\left(1+B_M\right)}{D_l \rho_l R_d} \left(Y_{li} - \varepsilon_i \right), \qquad (19)$$

$$\frac{\partial Y_{li}}{\partial R} \bigg|_{R=0} = 0, \qquad (20)$$

$$Y_{li}(t=0) = Y_{li0}(R), \qquad (21)$$

where

$$\varepsilon_i = \frac{Y_{vis}}{\sum_i Y_{vis}}, \qquad (22)$$

D_v is the vapour diffusion coefficient, B_M is the Spalding heat transfer number.

The analytical solution to (18) subject to the above-mentioned boundary and initial conditions, was implemented into the numerical code alongside the analytical solutions for temperature described in Section 2.2.

3. Numerical algorithm

The model described in Section 2 was implemented in the MATLAB R2020a code. 100 terms of the series in the analytical solutions for T_0 and T_1, and 200 terms of the series in the analytical solutions for Y_{li} were used. The timestep was taken equal to 0.1 s; 10,000 concentric spherical layers were used to calculate integrals over the distance from the droplet centre in the corresponding analytical solutions. The roots of the equations for eigen values were calculated using the bisection method with maximal absolute errors 10^{-12}.

The following steps were used in the numerical code.

1. Assume the initial distribution of temperature and mass fractions of the liquid components in the droplet, or use the distributions obtained at the end of the previous timestep. It was assumed that the initial distributions of temperature and mass fractions of components are homogeneous.

2. Calculate the partial pressures of components in the gas phase based on Raoult's law and the molar fractions of the components in the liquid phase using the initial distribution of components in the liquid phase or the one predicted by the analytical solution to (18) at the end of the previous timestep.

3. Calculate all the values of the liquid droplet thermophysical properties.

4. Calculate the droplet evaporation rate using the Abramzon and Sirgnano model [21].

5. Calculate the temperature distribution inside the droplet at the end of the timestep using the analytical solutions for T_0 and T_1.

6. Calculate the distribution of components inside the droplet at the end of the timestep using the analytical solutions for Y_{li}.

7. Calculate the change in the droplet radius due to swelling and evaporation; recalculate the value of the droplet radius at the end of the timestep.

8. Return to step 1 and repeat the calculations for the following timestep or complete calculations.

A schematic diagram of the numerical algorithm used in our analysis is presented in Fig. 1.

The numerical calculation of T_1 was based on Expression (49) (see Appendix D for the details of the derivation of this expression).

All three thermophysical properties (ρ_l, c_l and k_l) depend on temperature, while temperature depends on R. Taking this dependence from the previous timestep, we obtain ρ_l, c_l and k_l depending on R. We subtract average values of ρ_l, c_l and k_l from these parameters and arrive at the required perturbations ρ_{l1}, c_{l1} and k_{l1}.

4. Verification of the new algorithm

The predictions of the new algorithm were verified by comparing them with the results of a numerical simulation of heating and evaporation of a nanofluid (mixture of distilled water and SiO_2 nanoparticles) droplet obtained using the commercial COMSOL Multiphysics package. The input parameters used for the verification were the same as used in the experiments described in [20]. The mass fraction of SiO_2 nanoparticles was taken equal to 2%; the ambient gas temperature and initial droplet temperature were assumed equal to 28.4 °C; relative humidity was equal to 4.3%; air velocity was 0.2 m/s; the diameter of the holder was taken equal to 0.105 mm; the initial droplet diameter was equal to 2.19 mm.

The plots of average droplet temperature T_{av} and mass fraction of nanoparticles at the droplet surface $Y_{s,1}$ versus time predicted by the new algorithm and COMSOL Multiphysics for the above-mentioned values of input parameters are presented in Fig. 2. As can be seen from this figure, the plots predicted by both codes coincide within the accuracy of plotting. This gives us confidence in the new numerical algorithm.

Remembering that $T_1 \ll T_0$ in most engineering applications, the results of additional verification of the new code are presented in Fig. 3
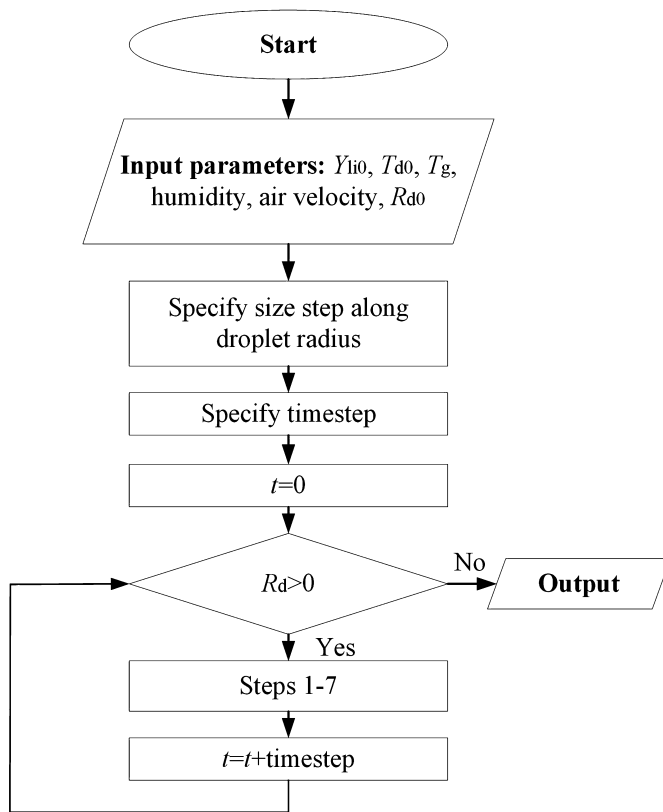
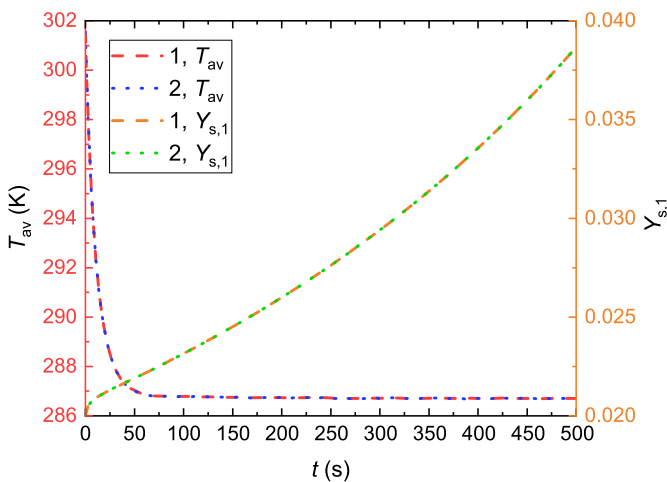**Fig. 1.** A schematic diagram of the numerical algorithm.

Fig. 2. Plots of average droplet temperature T_{av} and mass fraction of nanoparticles at the droplet surface $Y_{s,1}$ versus time for the input parameters described in Section 4. Plots 1 and 2 show the results predicted by the new algorithm and COMSOL Multiphysics, respectively.
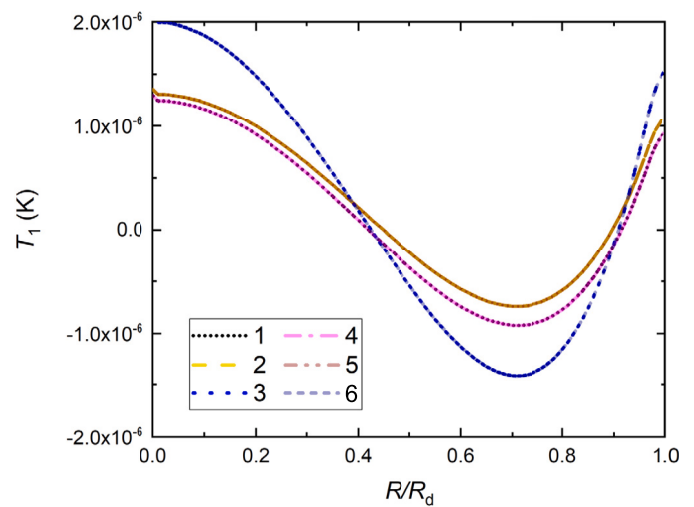

Fig. 3. Plots of T_1 predicted by the new algorithm and $T_1 = T_M - T_{M0}$ predicted by COMSOL Multiphysics versus normalised distance from the droplet centre at three time instants. T_M and T_{M0} are the distributions of temperature predicted by COMSOL Multiphysics taking into account the space distribution of thermophysical properties in the droplet, and assuming that these properties are constant during each timestep and equal to their average values, respectively. Curves 1, 2, and 3 show the predictions of the new algorithm, while Curves 4, 5, and 6 show the predictions of COMSOL Multiphysics. Curves 1 and 4 refer to time instant $t = 50$ s; Curves 2 and 5 refer to time instant $t = 100$ s; Curves 3 and 6 refer to time instant $t = 500$ s.

using the same input parameters as in Fig. 2. Firstly, we took into account the actual distribution of thermophysical properties in droplets (distribution of T_M). Secondly, we used thermophysical properties averaged over the whole droplet volume during each timestep (distribution of T_{M0}). The value of $T_M - T_{M0}$ in this case is T_1 predicted by COMSOL Multiphysics.

The results of comparison between the values of T_1 predicted by the new algorithm and COMSOL Multiphysics are presented in Fig. 3. As can be seen from this figure, the predictions of the new algorithm and COMSOL Multiphysics coincide within the accuracy of plotting. The predictions of both codes, presented in Figs. 2 and 3, differ by less than 0.01%, which justifies use of the new algorithm.

Note that the values of T_1 presented in Fig. 3 are several orders of magnitude lower than the values of T_0 presented in Fig. 2. This supports the key assumption of our model that $T_1 \ll T_0$.

5. Parametric study

In this section, the results of application of the model and numerical algorithm, described in Sections 2 and 3, to the analysis of cooling/heating of nanofluid (a mixture of distilled water and SiO_2 nanoparticles) droplets are described.

A nanofluide with SiO_2 nanoparticles of mass fraction 2% was prepared by adding these nanoparticles to distilled water [20]. Droplets were formed on the thread using a Thermo Scientific mechanical pipette with total errors of about ± 0.1 μl. Using infrared thermography, the droplet average temperature was determined (see Fig. 4). The measurements were performed with an NEC TH7102IR thermal imaging camera at wavelengths $\lambda = 8 - 14$ μm using a TH 71-377 macro lens. The droplet size dynamics were recorded by a Baumer vcxg-04m camera (720×540 pixels at a maximal speed of 431 fps). The photographs obtained were used to measure the diameters of droplets during evaporation (Fig. 4).

Firstly, we focus on the same experiments as described in Section 4. Droplet photographs and thermograms obtained in these experiments are shown in Fig. 4.

The plots of temperatures at the droplet surface (T_s) and centre (T_c) versus time at times up to 500 s, predicted by the new non-linear model and the model based on the assumption that all thermophysical properties are constant (linear model), are shown in Fig. 5. Note that the time limit of 500 s ensured that the droplet evaporation process did not reach the stage of cenosphere formation (which is expected to happen when the mass fraction of nanoparticles at the droplet surface reaches about 40% [20]). Droplet heating and evaporation after the cenosphere has been formed cannot be described by either non-linear or linear models.

As can be clearly seen in Fig. 5, the temperatures predicted by the non-linear and linear models practically coincide (they differ by less than 0.01%). This means that the linear heat conduction equation can
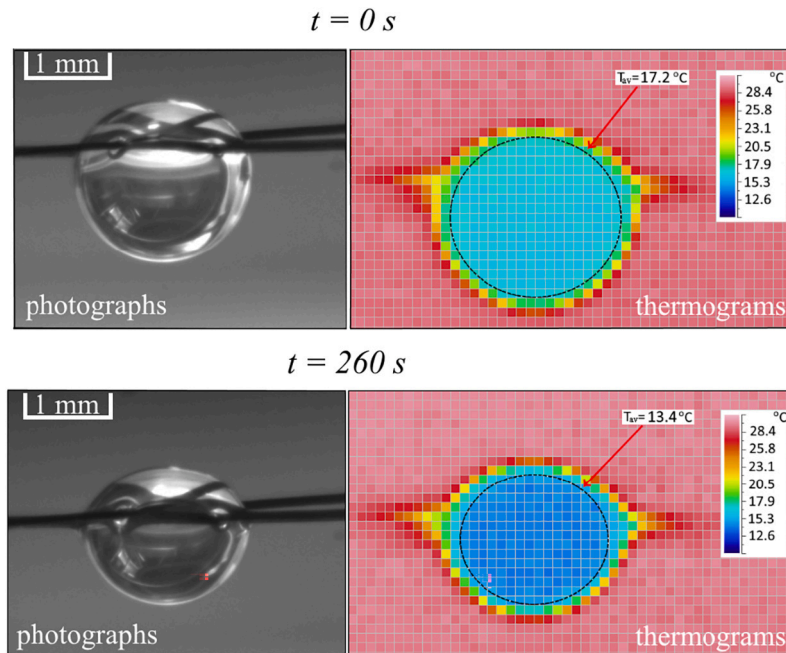
Fig. 4. Photographs (left) and thermal images (thermograms, right) of nanofluid droplets at the initial stage of their heating and evaporation (top) and at time instant 260 s (bottom). (For interpretation of the colours in the figure(s), the reader is referred to the web version of this article.)
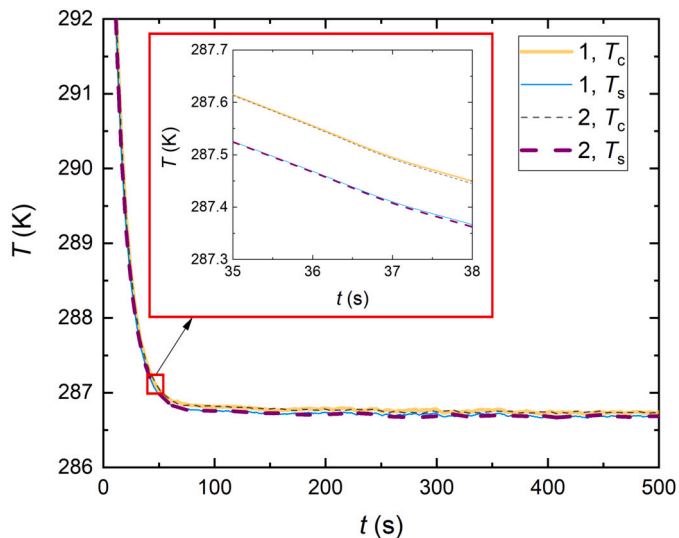

Fig. 5. Plots of temperatures at the droplet surface (T_s) and centre (T_c) versus time predicted by the linear (dashed) and non-linear (solid) models. The initial mass fraction of SiO_2 nanoparticles was taken equal to 2%; the ambient gas temperature and initial droplet temperature were assumed equal to 28.4 °C, the initial droplet diameter was taken equal to 2.19 mm. Zoomed parts of the curves are shown in the insert.

be used with confidence for the analysis of experimental results presented in [20].

To further investigate the effect of non-linearity on the solution to the heat transfer equation an extreme rather than typical case of heating of nanofluid droplets with initial diameter 10 mm in ambient gas at temperature 1000 K was considered. The initial mass fraction of SiO_2 nanoparticles was taken equal to 10%. All other parameters were the same as in the case shown in Fig. 5. The plots of temperatures at the droplet surface (T_s) and centre (T_c) versus time, predicted by the non-linear and linear models for this new case, are shown in Fig. 6.

As follows from Fig. 6, the temperatures predicted by the non-linear and linear models are close, as in the case shown in Fig. 5. At the same

time, the difference in temperatures predicted by both models is about 20 times larger for the case shown in Fig. 6 than in the case shown in Fig. 5, and reaches about 0.2%.

Note that relatively small differences in the temperatures predicted by both models lead to a much more noticeable difference in integral characteristics, such as time before the start of the formation of the cenosphere when the mass fraction of nanoparticles at the droplet surface reaches about 40%. In the case shown in Fig. 6 this time predicted by the non-linear model was 16.3 s, while that predicted by the linear model was 15.7 s. The difference between these times was more than 3.5%.

The difference between the predictions of both models is expected to be even more pronounced when the difference between the thermophysical properties of nanoparticles and liquid is larger than in the case of SiO_2 nanoparticles and water considered in [20]. A brief review of various nano-fluids is presented in [23].

6. Conclusions

A new analytical solution to a non-linear heat transfer equation in a spherically-symmetric droplet was suggested. The Robin boundary condition at the droplet surface was assumed. The non-linearity of this equation was considered to be weak, so that all thermophysical properties inside the droplet were considered to be close to the average values of these properties. The dependence of these properties on time was not considered. These assumptions allowed us to present the solution to the non-linear heat conduction equation as $T = T_0 + T_1$, where T_0 is the solution to a linear heat conduction equation (all thermophysical properties are assumed to be constant), and $T_1 \ll T_0$. The equation for T_1 was presented as a linear heat conduction equation with a source term depending on the distribution of T_0 and its spatial derivatives inside the droplet. The latter equation was solved analytically alongside the linear equation for T_0, and the final solution was presented as $T = T_0 + T_1$.

The new solution was implemented into a numerical MATLAB-based code and used at each timestep of the calculations. The solution at the end of the previous timestep was used as the initial condition for the current timestep with adjusted values of input parameters. Selecting sufficiently short timesteps ensured that the time dependence of thermophysical properties during the timestep could be safely ignored.
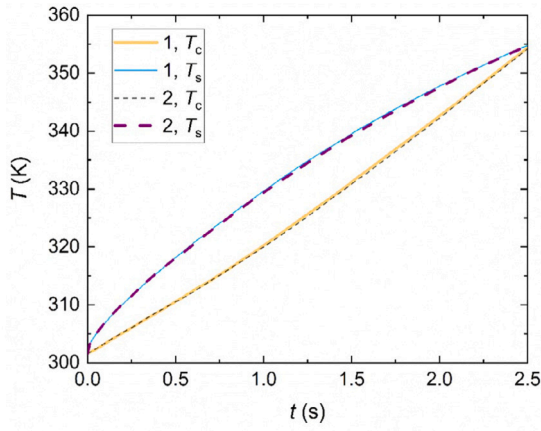
(a)
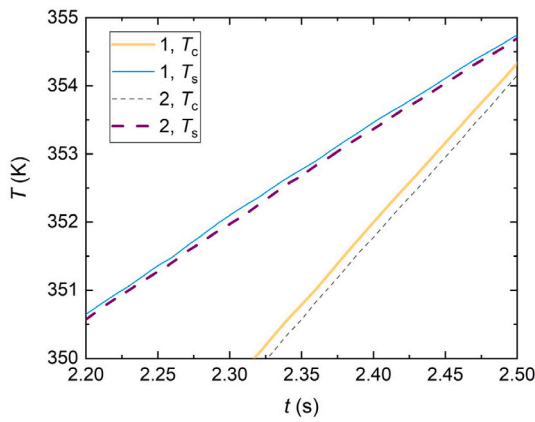
(b)

Fig. 6. (a) Plots of temperatures at the droplet surface (T_s) and centre (T_c) versus time predicted by the linear (dashed) and non-linear (solid) models. The mass fraction of SiO_2 nanoparticles was taken equal to 10%, the ambient gas temperature was assumed equal to 1000 K, and initial droplet temperature was assumed equal to 28.4 °C, the initial droplet diameter was taken equal to 5 mm. (b) Zoomed parts of the curves shown in Fig. 6a.

The predictions of the new numerical code were verified based on a comparison of its predictions with the predictions of COMSOL Multiphysics code using values of input parameters that are typical for nanofluid (water and SiO_2 nanoparticles) droplet evaporation in atmospheric conditions. It was demonstrated that for these experiments $T_1 \ll T_0$, which justifies the applicability of the linear heat conduction equation used for the analysis of this process. It was shown that small differences in the temperatures predicted by both non-linear and linear models lead to a much more noticeable difference in integral characteristics, such as time before the start of the formation of the cenosphere when the mass fraction of nanoparticles at the droplet surface reaches about 40%.

CRediT authorship contribution statement

Dmitrii V. Antonov: Investigation, Methodology, Resources, Software, Writing – review & editing. **Elena A. Shchepakina:** Investigation, Methodology, Resources, Writing – review & editing. **Vladimir A. Sobolev:** Investigation, Methodology, Resources, Writing – review & editing. **Elena M. Starinskaya:** Investigation, Resources. **Vladimir V. Terekhov:** Methodology, Resources. **Pavel A. Strizhak:** Methodology,

Resources. **Sergei S. Sazhin:** Conceptualization, Investigation, Methodology, Writing – original draft, Writing – review & editing.

Declaration of competing interest

Data availability

Data will be made available on request.

Acknowledgements

Appendix A

Following Expression (2.86) of [5], the solution to the heat conduction equation with a source term $P(R)$ can be presented as (using notations different from those used in [5]):

$$
\begin{aligned}
T = \frac{R_d}{R} \sum_{n=1}^{\infty} & \left\{ \frac{p_n}{\nu \mu_n^2} + \exp\left[-\nu \mu_n^2 t\right] \left(q_n - \frac{p_n}{\nu \mu_n^2} \right) \right. \\
& - \frac{2 A_n \sin \mu_n}{\mu_n^2} \mu_0(0) \exp\left[-\nu \mu_n^2 t\right] \\
& \left. - \frac{2 A_n \sin \mu_n}{\mu_n^2} \int_0^t \frac{d\mu_0(\tau)}{d\tau} \exp\left[-\nu \mu_n^2 (t - \tau)\right] d\tau \right\} \\
& \times \sin\left[\mu_n \left(\frac{R}{R_d}\right)\right] + T_g(t),
\end{aligned}
\tag{23}
$$

where μ_n are solutions to the equation

$$
\mu \cos \mu + b_0 \sin \mu = 0,
\tag{24}
$$

$$
\|v_n\|^2 = \frac{1}{2}\left(1 - \frac{\sin 2\mu_n}{2\mu_n}\right) = \frac{1}{2}\left(1 + \frac{b_0}{b_0^2 + \mu_n^2}\right),
$$

$$
q_n = \frac{1}{R_d \|v_n\|^2} \int_0^{R_d} T_0(R) \sin\left[\mu_n \frac{R}{R_d}\right] dR,
$$

$$
\nu = \frac{k_l}{c_l \rho_l R_d^2}, \quad \mu_0(t) = b T_g(t) R_d,
$$

$$b_0 = bR_d - 1, \quad T_0(R) = \frac{RT_{d0}(R)}{R_d}, \quad b = \frac{h}{k_l},$$

$$T_{d0}(R) = T(t = 0).$$

$$p_n = \frac{1}{R_d^2 \| v_n \|^2} \int_0^{R_d} R P(R) \sin\left(\mu_n R / R_d\right) dR.$$

The solution to Equation (8) follows from (23) if T_g in the latter expressions is replaced with

$$-\left[\frac{k_{l1}}{k_{l0}}\left[T_g(t) - T_0\right]\right]\Bigg|_{R = R_d - 0}.$$

The latter formula follows from the boundary condition (13).

Unfortunately, direct application of (23) for finding T_1 leads to serious numerical problems. The authors managed to overcome these problems by developing new analytical transformations described in Appendices B and D.

Appendix B

Consider an auxiliary equation

$$\frac{\partial u}{\partial t} = a^2 \left(\frac{\partial^2 u}{\partial R^2} + \frac{2}{R}\frac{\partial u}{\partial R}\right) + F(R,t) \tag{25}$$

with the boundary condition

$$\left(\frac{\partial u}{\partial R} + bu\right)\Bigg|_{R = R_d - 0} = bH(t) \tag{26}$$

and the initial condition

$$u(R, 0) = f(R). \tag{27}$$

Introducing the new function $v = u - H(t)$, Problem (25)-(27) is reduced to the problem:

$$\frac{\partial v}{\partial t} = a^2 \left(\frac{\partial^2 v}{\partial R^2} + \frac{2}{R}\frac{\partial v}{\partial R}\right) + \tilde{F}(R,t), \tag{28}$$

with the homogeneous boundary condition

$$\left(\frac{\partial v}{\partial R} + bw\right)\Bigg|_{R = R_d - 0} = 0 \tag{29}$$

and the initial condition

$$v(R, 0) = \tilde{f}(R), \tag{30}$$

where

$$\tilde{F}(R,t) = F(R,t) - \frac{dH(t)}{dt}, \quad \tilde{f}(R) = f(R) - H(0). \tag{31}$$

Following [24] we introduce new variable $vR = w$ and present Problem (28)-(30) as

$$\frac{\partial w}{\partial t} = a^2 \frac{\partial^2 w}{\partial R^2} + R\tilde{F}(R,t), \tag{32}$$

with the boundary condition

$$\left(\frac{\partial w}{\partial R} + b_1 w\right)\Bigg|_{R = R_d - 0} = 0, \quad b_1 = b - \frac{1}{R_d} \tag{33}$$

and the initial condition

$$w(R, 0) = R\tilde{f}(R). \tag{34}$$

The solution to the homogeneous equation

$$\frac{\partial w}{\partial t} = a^2 \frac{\partial^2 w}{\partial R^2} \tag{35}$$

subject to Conditions (33) and (34) can be presented as [24] (see pp. 237-238):

$$w(R,t) = \frac{2}{R_d} \sum_{n=1}^{\infty} A_n \sin\left(\mu_n \frac{R}{R_d}\right)$$

$$\times \exp\left(-\nu\mu_n^2 t\right) \int_0^{R_d} \sin\left(\mu_n \frac{r}{R_d}\right) r\tilde{f}(r) dr, \tag{36}$$

where

$$A_n = \frac{\mu_n^2 + (R_d b - 1)^2}{\mu_n^2 + R_d b(R_d b - 1)},$$

μ_n are solutions to Equation (24).

Formula (36) can be presented as [24]:

$$w(R,t) = \int_0^{R_d} G(R,r,t) r\tilde{f}(r) dr, \tag{37}$$

where

$$G(R,r,t) = \frac{2}{R_d} \sum_{n=1}^{\infty} A_n \sin\left(\mu_n \frac{R}{R_d}\right) \sin\left(\mu_n \frac{r}{R_d}\right) \exp\left(-\nu\mu_n^2 t\right) \tag{38}$$

is the Green function for Equation (35) with the boundary condition (33) and initial condition (34).

The solution to inhomogeneous Equation (32) can be presented as [25]:

$$w(R,t) = \int_0^{R_d} G(R,r,t) r\tilde{f}(r) dr$$

$$+ \int_0^t \int_0^{R_d} G(R,r,t-s) r\tilde{F}(r,s) dr ds. \tag{39}$$

Returning to the original variable $u = v + H(t) = (w/R) + H(t)$ we obtain:

$$u(R,t) = H(t) + \frac{1}{R} \int_0^{R_d} G(R,r,t) r\tilde{f}(r) dr$$

$$+ \frac{1}{R} \int_0^t \int_0^{R_d} G(R,r,t-s) r\tilde{F}(r,s) dr ds. \tag{40}$$

Remembering (31) we rewrite (40) as:

$$u(R,t) = Q(R,t) + \frac{1}{R} \int_0^{R_d} G(R,r,t) r f(r) dr$$

$$+ \frac{1}{R} \int_0^t \int_0^{R_d} G(R,r,t-s) r F(r,s) dr ds, \tag{41}$$

where

$$Q(R,t) = H(t) - \frac{1}{R} \int_0^{R_d} G(R,r,t) r H(0) dr$$

$$- \frac{1}{R} \int_0^t \int_0^{R_d} G(R,r,t-s) r \frac{dH(s)}{ds} dr ds. \tag{42}$$

Using formula

$$\int_0^{R_d} \sin\left(\mu_n \frac{r}{R_d}\right) r dr = \left(\frac{R_d}{\mu_n}\right)^2 (\sin(\mu_n) - \mu_n \cos(\mu_n))$$

$$= \left(\frac{R_d}{\mu_n}\right)^2 bR_d \sin(\mu_n),$$

we can write

$$\int_0^{R_d} G(R,r,t)r(-H(0))dr = -H(0)\frac{2}{R_d}\sum_{n=1}^{\infty} A_n\left(\frac{R_d}{\mu_n}\right)^2$$

$$\times bR_d\sin(\mu_n)\exp\left(-\nu\mu_n^2 t\right). \tag{43}$$

Note that

$$\int_0^t\int_0^{R_d} G(R,r,t-s)r\left(-\frac{dH(s)}{ds}\right)drds =$$

$$-\frac{2}{R_d}\sum_1^{\infty} A_n\sin\left(\mu_n\frac{R}{R_d}\right)\left(\frac{R_d}{\mu_n}\right)^2 bR_d\sin(\mu_n)$$

$$\times\int_0^t\frac{dH(s)}{ds}\exp\left(-\nu\mu_n^2(t-s)\right)ds = -2bR_d^2\sum_{n=1}^{\infty} A_n$$

$$\times\frac{\sin(\mu_n)}{\mu_n^2}\sin\left(\mu_n\frac{R}{R_d}\right)\int_0^t\frac{dH(s)}{ds}\exp\left(-\nu\mu_n^2(t-s)\right)ds. \tag{44}$$

Having substituted (44) and (43) into (42) we obtain:

$$Q(R,t) = H(t) - \frac{1}{R}H(0)\frac{2}{R_d}\sum_{n=1}^{\infty} A_n\left(\frac{R_d}{\mu_n}\right)^2\sin\left(\mu_n\frac{R}{R_d}\right)$$

$$\times bR_d\sin(\mu_n)\exp\left(-\nu\mu_n^2 t\right) - \frac{1}{R}2bR_d^2\sum_{n=1}^{\infty} A_n$$

$$\times\frac{\sin(\mu_n)}{\mu_n^2}\sin\left(\mu_n\frac{R}{R_d}\right)\int_0^t\frac{dH(s)}{ds}\exp\left(-\nu\mu_n^2(t-s)\right)ds. \tag{45}$$

Recalling that

$$\int_0^t f(s)dg(s) = f(s)g(s)\Big|_0^t - \int_0^t g(s)df(s)$$

$$= f(t)g(t) - f(0)g(0) - \int_0^t g(s)\frac{df(s)}{ds}ds,$$

the last integral in (45) can be rearranged to:

$$\int_0^t\frac{dH(s)}{ds}\exp\left(-\nu\mu_n^2(t-s)\right)ds = \int_0^t\exp\left(-\nu\mu_n^2(t-s)\right)dH(s) =$$

$$\exp\left(-\nu\mu_n^2(t-s)\right)H(s)\Big|_0^t - \int_0^t H(s)d\exp\left(-\nu\mu_n^2(t-s)\right) =$$

$$H(t) - H(0)\exp\left(-\nu\mu_n^2 t\right) - \nu\mu_n^2\int_0^t H(s)\exp\left(-\nu\mu_n^2(t-s)\right)ds.$$

Hence, an alternative expression for $Q(R,t)$ is obtained:

$$Q(R,t) = H(t) - \frac{2}{RR_d}\sum_{n=1}^{\infty} A_n\sin\left(\mu_n\frac{R}{R_d}\right)\left(\frac{R_d}{\mu_n}\right)^2 bR_d\sin(\mu_n)$$

$$\times\left[H(t) - \nu\mu_n^2\int_0^t H(s)\exp\left(-\nu\mu_n^2(t-s)\right)ds\right]. \tag{46}$$

Expression (46) is expected to be more attractive for practical applications as it does not require differentiability of $T_g(t)$.

Appendix C

Assuming that $P = 0$, Expression (23) can be presented as:

$$T(R,t) = \tilde{Q}(R,t) + \frac{R_d}{R}\sum_{n=1}^{\infty} q_n\exp\left[-\nu\mu_n^2 t\right]\sin\left\{\mu_n\frac{R}{R_d}\right\}, \tag{47}$$

where

$$\tilde{Q}(R,t) = T_g(t) - \frac{R_d}{R}\sum_{n=1}^{\infty}\left\{\frac{2A_n\sin\mu_n}{\mu_n^2}\mu_0(0)\exp\left[-\nu\mu_n^2 t\right]\right.$$

$$\left. + \frac{2A_n\sin\mu_n}{\mu_n^2}\int_0^t\frac{d\mu_0(\tau)}{d\tau}\exp\left[-\nu\mu_n^2(t-\tau)\right]d\tau\right\}\sin\left\{\mu_n\frac{R}{R_d}\right\},$$

$$\mu_0(t) = bR_d T_g(t).$$

On the other hand, Expression (45) for $Q(R,t)$ can be presented as:

$$Q(R,t) = T_g(t) - \frac{2R_d^2 b}{R}\sum_{n=1}^{\infty} A_n\frac{\sin(\mu_n)}{\mu_n^2}\sin\left(\mu_n\frac{R}{R_d}\right)$$

$$\times\left\{T_g(0)\exp\left(-\nu\mu_n^2 t\right) + \right.$$

$$\left.\int_0^t\frac{dT_g(s)}{ds}\exp\left(-\nu\mu_n^2(t-s)\right)ds\right\}.$$

We can see that $\tilde{Q}(R,t) = Q(R,t)$. Also, we can see that the last terms on the right hand sides of Expressions (47) and (16) coincide. Hence Expression (23) with $P = 0$ is identical to Expression (16).

Appendix D

Remembering that $F(r,s)$ does not depend on s, i.e., $F(r,s) = F(r)$, and using the relationship

$$\int_0^t\exp\left(-\nu\mu_n^2(t-s)\right)ds = \left(\frac{R_d}{a\mu_n}\right)^2\left(1 - \exp\left(-\nu\mu_n^2 t\right)\right)$$

the double integral in (41) can be simplified to

$$\frac{1}{R}\int_0^t\int_0^{R_d} G(R,r,t-s)rF(r)drds =$$

$$\frac{1}{R}\int_0^t\int_0^{R_d}\frac{2}{R_d}\sum_1^{\infty} A_n\sin\left(\mu_n\frac{R}{R_d}\right)\sin\left(\mu_n\frac{r}{R_d}\right)\exp\left(-\nu\mu_n^2 t\right)rF(r)drds =$$

$$\frac{1}{R}\int_0^{R_d}\frac{2}{R_d}\sum_1^{\infty} A_n\sin\left(\mu_n\frac{R}{R_d}\right)\sin\left(\mu_n\frac{r}{R_d}\right)rF(r)\left[\int_0^t\exp\left(-\nu\mu_n^2 t\right)ds\right]dr =$$

$$\frac{1}{R}\int_0^{R_d}\frac{2}{R_d}\sum_1^{\infty} A_n\sin\left(\mu_n\frac{R}{R_d}\right)\sin\left(\mu_n\frac{r}{R_d}\right)rF(r)$$

$$\times\left[\left(\frac{R_d}{a\mu_n}\right)^2\left(1 - \exp\left(-\nu\mu_n^2 t\right)\right)\right]dr =$$

$$\frac{1}{R}\frac{2}{R_d}\sum_1^{\infty} A_n\left[\left(\frac{R_d}{a\mu_n}\right)^2\left(1 - \exp\left(-\nu\mu_n^2 t\right)\right)\right]\sin\left(\mu_n\frac{R}{R_d}\right)$$

$$\times\int_0^{R_d}\sin\left(\mu_n\frac{r}{R_d}\right)rF(r)dr.$$

Taking into account that

$$H(t) = H_1(t) = -\left\{\frac{k_{l1}}{k_{l0}}\left[T_g(t) - T_0\right]\right\}\Bigg|_{R=R_d-0}, \quad b = h/k_{l0}$$

we obtain the following expression for T_1:

$$T_1(R,t) = Q_1(R,t) + \frac{1}{R}\int_0^t\int_0^{R_d} G(R,r,t-s)r\frac{P(r)}{\rho_{l0}c_{l0}}drds, \tag{48}$$

where

$$Q_1(R,t) = H_1(t) - \frac{2}{RR_d} \sum_1^\infty A_n \sin\left(\mu_n \frac{R}{R_d}\right) \left(\frac{R_d}{\mu_n}\right)^2 bR_d \sin(\mu_n) \Bigg[H_1(t)$$

$$-\nu\mu_n^2 \int_0^t H_1(s) \exp\left(-\nu\mu_n^2(t-s)\right) ds \Bigg].$$

Formula (48) can be rewritten as

$$T_1(R,t) = Q_1(R,t) +$$

$$\frac{1}{R} \frac{2}{R_d} \sum_1^\infty A_n \left[\left(\frac{R_d}{a\mu_n}\right)^2 \left(1 - \exp\left(-\nu\mu_n^2 t\right)\right) \right] \sin\left(\mu_n \frac{R}{R_d}\right)$$

$$\times \int_0^{R_d} \sin\left(\mu_n \frac{r}{R_d}\right) r \frac{P(r)}{\rho_{l0} c_{l0}} dr$$

$$= Q_1(R,t) + \frac{2}{R_d} \sum_1^\infty A_n \left[\left(\frac{R_d}{a\mu_n}\right)^2 \left(1 - \exp\left(-\nu\mu_n^2 t\right)\right) \right] \frac{\mu_n}{R_d} \Phi(R,\mu_n)$$

$$\times \int_0^{R_d} \sin\left(\mu_n \frac{r}{R_d}\right) r \frac{P(r)}{\rho_{l0} c_{l0}} dr,$$

where

$$\Phi(R,\mu_n) = \sin\left(\mu_n \frac{R}{R_d}\right) \Bigg/ \left(\mu_n \frac{R}{R_d}\right).$$

This leads to the final expression for $T_1(R,t)$ which was used in the numerical code:

$$T_1(R,t) = Q_1(R,t) + \frac{2}{k_{l0}} \sum_1^\infty A_n \frac{1}{\mu_n} \left[1 - \exp\left(-\nu\mu_n^2 t\right)\right] \Phi(R,\mu_n)$$

$$\times \int_0^{R_d} \sin\left(\mu_n \frac{r}{R_d}\right) rP(r) dr. \tag{49}$$

References

[1] N. Fuchs, Evaporation and Droplet Growth in Gaseous Media, Pergamon Press, 1959.
[2] D. Spalding, Convective Mass Transfer; an Introduction, Edward Arnold Ltd, London, 1963.
[3] W. Sirignano, Fluid Dynamics and Transport of Droplets and Sprays, second edition, Cambridge University Press, 2010.
[4] G. Cossali, S. Tonini, Drop Heating and Evaporation: Analytical Solutions in Curvilinear Coordinate Systems, Springer, 2021.
[5] S.S. Sazhin, Droplets and Sprays: Simple Models of Complex Processes, Springer, 2022.
[6] H. Erbil, Evaporation of pure liquid sessile and spherical suspended drops: a review, Adv. Colloid Interface Sci. 170 (2012) 1–2.
[7] R. Deb, I. Khan, S. Sundriyal, A review of evaporation droplets on a transparent heater, Mater. Today Proc. 90 (2023), https://doi.org/10.1016/j.matpr.2023.02.119.
[8] A. Dahale, E. Pomraning, Modeling spherical droplet evaporation using a shell based approach, in: Proceedings of ILASS-Americas 33rd Annual Conference on Liquid Atomization and Spray Systems, May 14–17, 2023, 2023.
[9] S. Utyuzhnikov, Numerical modeling of combustion of fuel-droplet-vapour releases in the atmosphere, Flow Turbul. Combust. 68 (2002) 137–152.
[10] A. Pinheiro, J. Vedovoto, Evaluation of droplet evaporation models and the incorporation of natural convection effects, Flow Turbul. Combust. 102 (2019) 537–558.
[11] D. Antonov, S. Tonini, G. Cossali, V. Dolgikh, P. Strizhak, S. Sazhin, Droplet heating and evaporation: a new approach to the modelling of the processes, Phys. Fluids 35 (2023) 073311.
[12] S. Tonini, G. Cossali, An analytical model of liquid drop evaporation in gaseous environment, Int. J. Therm. Sci. 57 (2012) 45.
[13] E. Shchepakina, V. Sobolev, M. Mortell, Singular Perturbations: Introduction to System Order Reduction Methods with Applications, Springer, 2014.
[14] G. Schneider, H. Uecker, Nonlinear PDEs: A Dynamical Systems Approach, American Mathematical Society, 2017.
[15] M. Becker, Nonlinear transient heat conduction using similarity groups, J. Heat Transf. 122 (1) (2000) 33–39.
[16] J. Parlange, W. Hogarth, M. Parlange, R. Haverkamp, D. Barry, P. Ross, T. Steenhuis, Approximate analytical solution of the nonlinear diffusion equation for arbitrary boundary conditions, Transp. Porous Media 30 (1) (1998) 45–55.
[17] P. Thakare, V. Nair, K. Sinhai, A weakly nonlinear framework to study shock–vorticity interaction, J. Fluid Mech. 933 (2022) A48.
[18] A. Luikov, Analytical Heat Diffusion Theory, Academic Press, New York, 1968.
[19] A. Polyanin, Handbook of Linear Partial Differential Equations for Engineers and Scientists, Chapman & Hall, Boca Raton, 2002.
[20] E. Starinskaya, N. Miskiv, A. Nazarov, V.V. Terekhov, V.I. Terekhov, V. Rybdylova, S.S. Sazhin, Evaporation of suspended nanofluid (SiO_2/water) droplets: experimental results and modelling, Int. J. Thermophys. 44 (2023) 64.
[21] B. Abramzon, W. Sirignano, Droplet vaporization model for spray combustion calculations, Int. J. Heat Mass Transf. 32 (1989) 1605–1618.
[22] P. Strizhak, R. Volkov, G. Castanet, F. Lemoine, O. Rybdylova, S.S. Sazhin, Heating and evaporation of suspended water droplets: experimental studies and modelling, Int. J. Heat Mass Transf. 127 (2018) 92–106.
[23] S. Rashidi, N. Karimi, O. Mahian, J. Esfahani, A concise review on the role of nanoparticles upon the productivity of solar desalination systems, J. Therm. Anal. Calorim. 135 (2019) 1145–1159.
[24] H. Carslaw, J. Jaeger, Conduction of Heat in Solids, second edition, Clarendon Press, Oxford, 1959.
[25] K. Cole, J. Beck, A. Haji-Sheikh, B.B. Litkouhi, Heat Conduction Using Green's Functions, Taylor & Francis, 2010.